Available online at www.sciencedirect.com
ScienceDirect
Bioorganic & Medicinal Chemistry Letters 18 (2008) 2959–2966
Bioorganic & Medicinal Chemistry Letters

The design and synthesis of diaryl ether second generation HIV-1 non-nucleoside reverse transcriptase inhibitors (NNRTIs) with enhanced potency versus key clinical mutations

Thomas J. Tucker,[a,*] Sandeep Saggar,[a] John T. Sisko,[a] Robert M. Tynebor,[a] Theresa M. Williams,[a] Peter J. Felock,[b] Jessica A. Flynn,[c] Ming-Tain Lai,[b] Yuexia Liang,[d] Georgia McGaughey,[a] Meiquing Liu,[b] Mike Miller,[b] Gregory Moyer,[c] Vandna Munshi,[b] Rebecca Perlow-Poehnelt,[a] Sridhar Prasad,[a] Rosa Sanchez,[d] Maricel Torrent,[a] Joseph P. Vacca,[a] Bang-Lin Wan[a] and Youwei Yan[a]

[a]*Departments of Medicinal Chemistry and Structural Biology, Merck Research Laboratories, WP14-3, 770 Sumneytown Pike, PO Box 4, West Point, PA 19486-0004, USA*
[b]*Department of Antiviral Research, Merck Research Laboratories, WP14-3, 770 Sumneytown Pike, PO Box 4, West Point, PA 19486-0004, USA*
[c]*Department of Vaccines and Biologics Research, Merck Research Laboratories, WP14-3, 770 Sumneytown Pike, PO Box 4, West Point, PA 19486-0004, USA*
[d]*Department of Drug Metabolism, Merck Research Laboratories, WP14-3, 770 Sumneytown Pike, PO Box 4, West Point, PA 19486-0004, USA*

Received 31 January 2008; revised 20 March 2008; accepted 21 March 2008
Available online 25 March 2008

Abstract—Using a combination of traditional Medicinal Chemistry/SAR analysis, crystallography, and molecular modeling, we have designed and synthesized a series of novel, highly potent NNRTIs that possess broad antiviral activity against a number of key clinical mutations.

Since their discovery in the early 1990s, non-nucleoside reverse transcriptase inhibitors (NNRTIs) have been shown to be a key component of highly active anti-retroviral therapy (HAART). These compounds target an allosteric binding pocket that lies close to the catalytic site, and their binding is non-competitive with respect to dNTP's and template/primer.[1] There are currently three commercially available NNRTIs: efavirenz, nevirapine, and delavirdine (Fig. 1). The use of efavirenz and nevirapine has become a part of standard combination antiviral therapies producing clinical outcomes with efficacy comparable to other antiviral regimens.[2] Despite the demonstrated clinical efficacy of combination antiviral regimens using NNRTIs, the emergence of clinical resistance has become a key issue for this class of compounds and has become a major cause of treatment failure. A number of important resistant variants have

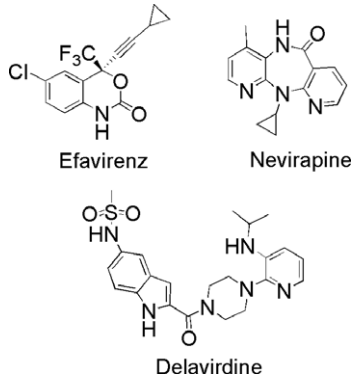

Figure 1. Currently marketed NNRTIs.

Keywords: NNRTI; HIV; Mutations.
* Corresponding author. Tel.: +1 215 699 3437; fax: +1 215 652 3971; e-mail: tom_tucker@merck.com

0960-894X/$ - see front matter © 2008 Elsevier Ltd. All rights reserved.
doi:10.1016/j.bmcl.2008.03.064

emerged, with the Lys103Asn (K103N) mutation conferring clinical resistance to most known NNRTIs and the Tyr181Cys (Y181C) mutation conferring clinical resistance to nevirapine.[2] Therefore, an urgent need has arisen for NNRTIs that possess both a broad spectrum of antiviral activity against key mutant strains and a high genetic barrier to the selection of new mutant strains. Using a combination of traditional Medicinal Chemistry/SAR analysis, molecular modeling, and crystallographic studies, we have designed and synthesized a series of novel, highly potent NNRTIs that possess broad spectrum antiviral activity. In this manuscript, we describe the design, synthesis, and biological profile of this series of novel NNRTIs.

Our early efforts in this series focused on the synthesis of analogs of **1** (Fig. 2), which were discovered by high throughput screening.[3] However, disappointing pharmacokinetic results with compounds of this class forced us to retarget our efforts.[3] Using **1** as a lead structure, and comparing the compound with the known NNRTI **2** (Fig. 2)[4] via a molecular modeling analysis,[5] we proposed to hold the common features of the two compounds constant and replace the western (A ring) portion of **2** with a novel biaryl sub-structure. Using a rapid analog approach, we examined a number of biaryl replacements, arriving at the novel diphenyl ether substructure of **3** (Fig. 2) that became a next generation lead for further efforts in our project. Direct molecular modeling comparison of **2** and **3** (Fig. 3)[5] suggested that the biaryl regions of the two molecules likely fit the NNRTI site in a highly similar manner, and also suggested that the amide carbonyl of **3** likely maintained a critical hydrogen bonding interaction with the backbone NH of Lysine 103 similar to that seen with **2**.[5] It is thought that direct interaction with the backbone of Lysine 103 is critical for maintaining good potency against mutations at this position such as K103N.[6] This modeling comparison strongly suggested (by analogy to **2**[5]) that the addition of di-meta substitution on the western aryl ring (A ring) as well as a 2 or 3 substituent on the central aryl ring (B ring) of **3** might help to optimize interactions with the binding site and help to further improve potency in this series. The model further suggested that the aryl sulfonamide eastern ring (C ring) lied along the enzyme/water interface with the sulfonamide group fully

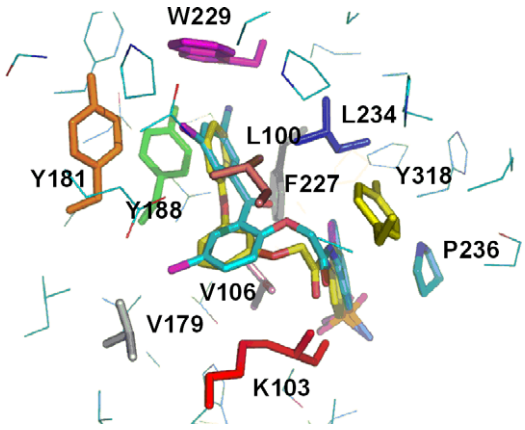

Figure 3. Molecular modeling comparison of compound **2** (blue) and compound **3** (yellow) in the WT-NNRTI binding site. Key active site residues are labeled in black. Details of the molecular modeling methodologies are provided in Ref. 5.

solvent exposed, indicating the potential for various polar substitutions in this region. Using this modeling study as a guide, we moved forward to prepare a series of analogs of **3** in an effort to enhance the potency of this series.

Analogs in this series were synthesized via the route detailed in Scheme 1.[7] The lead structure **3** was prepared via a two-step synthesis. Acylation of aniline **4** with acid bromide **5** provided the alpha-bromo amide intermediate **6**. Alkylation of 3-phenoxyphenol with **6** provided **3** in low yield. S_NAR reaction of the commercially available phenols **7** and fluoride **8** provided the diaryl ether intermediates **9** in good yield. The methyl protecting group of intermediates **9** was removed in nearly quantitative yield by treatment with boron tribromide to give the key diaryl ether–phenol intermediate **10**. Alkylation of **10** with *tert*-butyl bromoacetate provided the *tert*-butyl ester, which was cleaved with TFA and the crude acid refluxed with thionyl chloride to provide the acid chloride **11** in 40% yield for the three step transformation. Treatment of the acid chloride with the requisite aniline derivative in refluxing benzene gave the desired amide derivatives **12**–**17** in moderate to good yield. Alternatively, the key phenol intermediate **10** was alkylated with the desired chloromethyl or bromomethyl

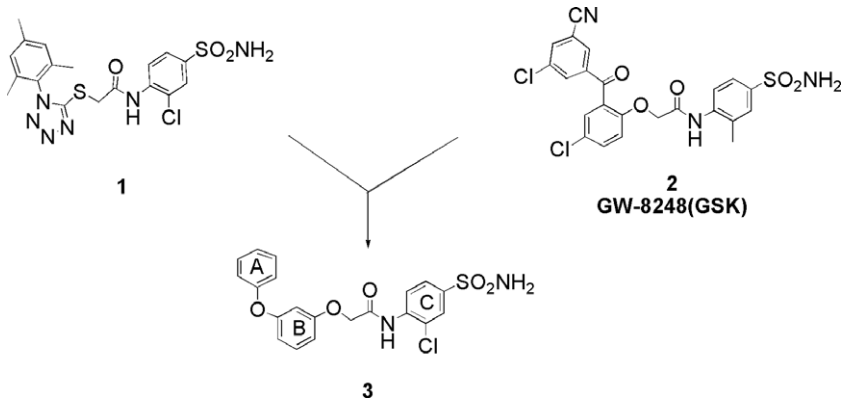

Figure 2. Design paradigm for novel diaryl ether lead structures.

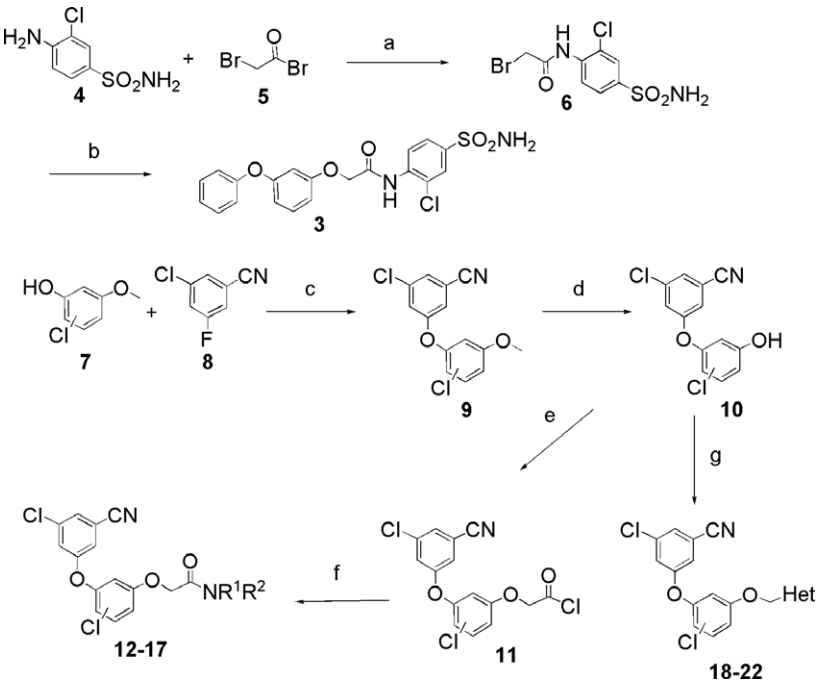

Scheme 1. Synthesis of amide analogs **3**, **12**–**17** and heterocyclic analogs **18**–**22**. Reagents and conditions: (a) $NaHCO_3$, CH_2Cl_2, rt (88%); (b) NaH, 2-phenoxyphenol DMF, rt, 2 h (20%); (c) K_2CO_3, NMP, 120° (75%); (d) BBr_3, CH_2Cl_2 (95%); (e) i—NaH, *tert*-butylbromoacetate, DMF; ii—neat TFA; iii—$SOCl_2$/reflux (40% for the three steps); (f) HNR^1R^2, benzene, reflux overnight (30–90%); (g) i—NaH, XCH_2Het, DMF, 2–4 h; ii—deprotection (if needed) (70–90% for two steps). Full experimental details and analytical data are provided in Ref. 7.

heterocycle derivative (purchased commercially or prepared according to standard literature methods) to provide the desired heterocyclic products **18**–**22**. In the case of the indazole derivative **22**, it was necessary to use the N1-Boc protected 3-bromomethyl indazole in the alkylation, and the Boc protected product was treated with neat TFA to remove the Boc group and provide **22**.

Table 1 details the data for the amide series of analogs. Compounds were evaluated for intrinsic enzyme inhibitory potency versus WT RT (wild type HIV-1 reverse transcriptase), as well as the K103N and Y181C mutant RTs.[8] Compounds were also evaluated for antiviral potency (CIC_{95}) against WT and the key mutant viruses in the presence of 10% FBS (Fetal Bovine Serum; WT and mutants) as well as 50% NHS (Normal Human Serum; WT) to evaluate the effects of protein binding.[9] Adding the 3-chloro substituent to the central aryl ring (**12**) resulted in an increase in activity versus WT and the Y181C mutant RT enzyme. Addition of a meta cyano substituent to the A ring resulted in a large enhancement of potency (**13**) versus WT and both the K103N and Y181C enzymes, and the further addition of a second meta chloro substituent provided a more moderate enhancement in potency versus the K103N mutant (**14**). This di-meta substitution on the A ring appears to provide excellent potency versus WT and the key mutant enzymes, similarly to the SAR seen with **2**.[4] Crystallographic studies with **14** (Fig. 4)[10] confirmed the predictions of our earlier molecular modeling studies. The crystal structure of **14**[10] demonstrated (as suggested by the modeling study depicted in Fig. 3) that the A ring was indeed filling the large lipophilic Y181–Y188–W229 binding pocket of the NNRTI site, while the chlorine atom on the central ring fit tightly in a small lipophilic pocket below the Y181 residue and behind V179. The Y181 side chain is rotated by approximately 90° relative to its position in most first generation NNRTI crystal structures,[6] and is sandwiched between the meta chlorine atom of the A western ring and the 3-chlorine atom of the central B ring. The observed rotation of the Y181 side chain may be important for attaining the high levels of potency versus the Y181C mutant seen with this series, as the direct stacking interaction between the A ring of the inhibitor and the aryl ring of the Y181 side chain is minimized. In some first generation NNRTIs such as nevirapine, this pi-stacking interaction is critical for attaining potency but becomes a key liability versus the Y181C mutant.[6] The amide carbonyl group of the inhibitor makes a direct H-bonding interaction with the backbone NH of K103, another key interaction that contributes to the high levels of potency observed against the K103N mutation. The C ring and its *ortho*-chlorine substituent make lipophilic interactions with Y318, F227, P236, and V106. The entire eastern edge of the C ring lies along the solvent interface, with the 4-sulfonamide group completely solvent exposed. The crystal structure suggested that moving the chlorine atom on the B ring to the neighboring 2-position might provide an even better fit in the active site, since the chlorine atom of **14** appeared to be making very close contact with the side chain of V179. Moving the 3-chlorine substituent on the central aryl B ring one position to the 2-position (**15**) resulted in an increase in potency versus WT and the key mutant enzymes, providing a compound with sub-nanomolar enzyme inhibitory potency and high levels of antiviral potency in our cell based assay. Replacement of the aryl sulfonamide of **15** with a

Table 1. Data for reference compounds **1**–**2** and amide derivatives **3**, **12**–**17**

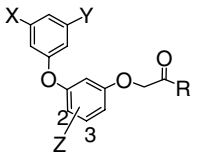

3, 12-17

Compound	X	Y	Z	R	Inhibition of RT polymerase, IC_{50} (nM)[a]			Antiviral activity in cell culture, CIC_{95} (nM)[b]			
					WT	K103N	Y181C	WT (10% FBS)	K103N (10% FBS)	Y181C (10% FBS)	WT (50% NHS)
1	—	—	—	—	4.05	10.37	34.52	16	ND	ND	62
2	—	—	—	—	2.16	3.16	2.48	2.65	6.98	3.28	30.48
3	H	H	H	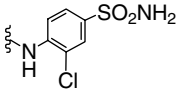	51.70	192.4	722	ND	ND	ND	ND
12	H	H	3-Cl	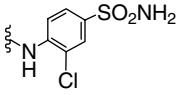	10.50	218	25	ND	ND	ND	ND
13	H	CN	3-Cl	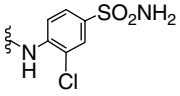	0.96	14.4	1.2	8	ND	ND	160
14	Cl	CN	3-Cl	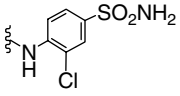	2.11	3.48	2.66	16	ND	ND	125
15	Cl	CN	2-Cl	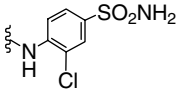	0.14	0.21	0.28	7.56	9.52	14.85	23.91
16	Cl	CN	2-Cl	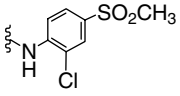	0.99	1.33	0.91	31	ND	ND	78
17	Cl	CN	2-Cl	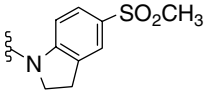	0.86	0.33	1.7	3.68	5.26	14.26	29.74

[a] Compounds were evaluated in a standard SPA assay. Values are the geometric mean of at least two determinations. ND, not determined. Assay protocols are detailed in Ref. 8.

[b] CIC_{95} (Cell culture inhibitory concentration) is defined as the concentration at which the spread of virus is inhibited by >95% in MT-4 human T-lymphoid cells maintained in RPMI 1640 medium containing either 10% FBS or 50% NHS. Details of the assay protocols are provided in Ref. 9. Values are the geometric mean of at least two determinations. ND, not determined. No cytotoxicity was observed for any of the compounds up to the upper limit of the assay (8.3 μM).

methyl sulfone provided **16**, which was essentially equipotent with **15**. Unfortunately, **15** and **16** are rapidly cleared in rats and dogs after iv administration, and metabolic profiling confirmed that the anilide underwent rapid metabolic hydrolysis.[11]

In an effort to prevent the metabolic hydrolysis of this critical amide, we examined cyclic amide derivatives. Cyclization from the *ortho* position of the aromatic ring back to the nitrogen of the amide appeared to be a reasonable approach, allowing the aliphatic carbons to fill the same space as the chloro substituent, while also allowing the amide carbonyl to maintain the key hydrogen bonding interaction with the NH of K103. The cyclic amide analog **17** (Table 1) retained excellent intrinsic and cell based potency, and showed enhanced stability, longer half-live and lowered clearance after iv dosing to rats and dogs.[11] Unfortunately, the compound also

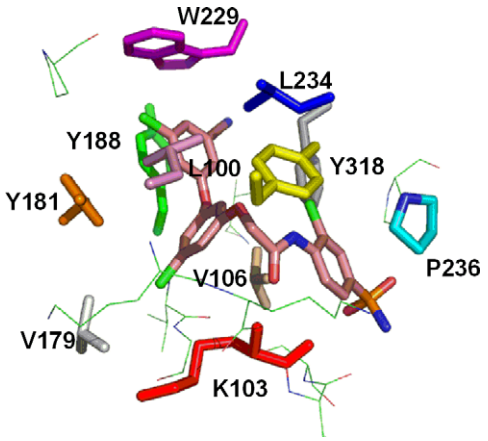

Figure 4. The X-ray crystal structure of compound **14** (salmon) bound to the NNRTI binding site (2.7 Å resolution). Details of the crystallographic studies are provided in Ref. 10.

showed low oral bioavailability in both rats and dogs (<3%), and had low solubility.

Given the issues we had encountered with amides **12**–**17** (Table 1), we proceeded to alter the structure to obtain compounds with more favorable profiles. We hypothesized that it might be possible to replace the C-ring amide portion of the molecules with a series of heterocycles that would use a heteroatom to maintain the key hydrogen bond acceptor role of the amide carbonyl (Fig. 5).[12] Replacement of the amide functionality with a series of heterocycles provided **18**–**22** (Table 2). The simple benzthiazole analog **18** showed somewhat reduced but still encouraging enzyme potency in comparison to the previously prepared amide analogs. Addition of the chlorine atom (**19**) to mimic the chlorine of the amide series resulted in an increase in enzyme potency; however, antiviral potency remained low. The compound was shifted in the presence of 50% NHS, suggesting high levels of protein binding. In an effort to lower the lipophilicity and protein binding of these compounds, the benzoxazole analog **20** was prepared, and showed excellent enzyme potency; however, the modest cell based potency remained an issue. Moving to the more polar benzimidazole core (**21**) provided a compound with enhanced physical properties. However, the more polar heterocyclic nucleus was not well tolerated by the enzyme active site, leading to losses in enzyme and antiviral potency. Interestingly, **21** showed moderate clearance (13.6 ml/min/kg) and a long half life (10.8 h) after iv dosing in rats.[11] These results taken in combination suggested that there was indeed some viability to the concept of replacing the amide functionality with a heterocycle, however, it was clear that more potency and solubility combined with less lipophilicity would be needed to make molecules of this type attractive for further investigation. In an effort to develop novel amide replacements with better physical properties and the potential for increased potency, we began to look toward other heterocyclic motifs that might be suitable as replacements for the aryl amide. After careful consideration of the modeling and crystallographic data, we rationalized that an indazole moiety (Fig. 6) might provide a novel replacement for this region of the molecule. The indazole nucleus would have the added potential of making two hydrogen bonding interactions with both the backbone NH and the backbone carbonyl of K103 while maintaining many of the lipophilic interactions provided by the aryl amide moiety. Incorporation of the indazole moiety into the molecule provided **22** (Table 2), which showed high levels of enzyme and cell-based potency. Compound **22** (Table 3) demonstrated moderate pharmacokinetics after iv dosing to rats, dogs, and rhesus macaques and showed low levels of oral bioavailability after dosing in rats. Various manipulations of the dosing vehicle formulation have enhanced this number to 10%, however, this is still less than desired for further development. The compound possesses low solubility which appears to be responsible for the low oral bioavailability. Compound **22** was also evaluated for its antiviral potency versus a panel of clinical mutations[13] (Table 4) in the presence of 40% NHS, and was shown to possess broad potency versus most of the mutations tested. Only the rare mutation Y188L (occurs in 0.6% of clinical isolates)[14] provided notable decreases in potency; this is presumably due to the intimate interaction between the Western A ring of **22** and the aryl ring of the Y188 residue. When the residue is mutated to a leucine, much of the interaction between the inhibitor A ring and the sidechain is lost due to the decreased size of the sidechain as well as the loss of the pi-stacking interaction. Crystallographic studies with **22** (Fig. 7)[15] confirmed the binding mode proposed earlier (Fig. 6) for the compound. All of the key lipophilic interactions of the western A ring and central B ring are maintained as in previous compounds. The Y181 side chain is rotated by 90° as seen in the earlier crystal structure of **14**. As theorized, the two pyrrolo nitrogens of the indazole moiety appear to make two direct hydrogen bonding interactions with the NH and carbonyl of

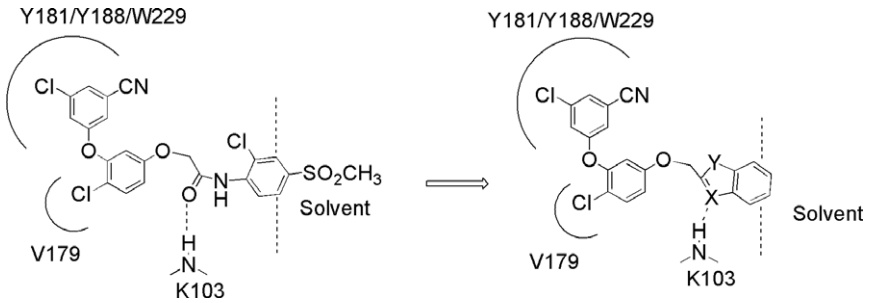

Figure 5. Proposed binding mode for heterocyclic derivatives **18**–**21**.

Table 2. SAR for heterocyclic derivatives **18–22**

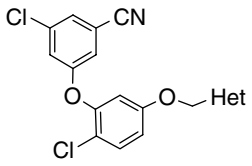

18-22

Compound	Het	Inhibition of RT polymerase, IC_{50} (nM)[a]			Antiviral activity in cell culture, CIC_{95} (nM)[b]			
		WT	K103N	Y181C	WT(10% FBS)	K103N(10% FBS)	Y181C(10% FBS)	WT(50% NHS)
18	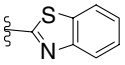	19.29	79.24	54.92	312	ND	ND	1250
19	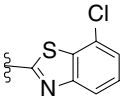	3.06	5.98	5.15	156	ND	ND	1250
20	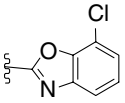	0.59	1.41	6.38	78	ND	ND	312
21	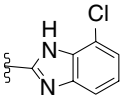	3.2	7.30	50	103	ND	ND	2778
22	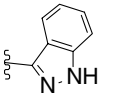	1.35	1.12	2.62	22.57	33.44	101.5	114.4

[a] Compounds were evaluated in a standard SPA assay; values are the geometric mean of multiple determinations. ND, not determined. Assay protocols are detailed in Ref. 8.

[b] CIC_{95} (Cell culture inhibitory concentration) is defined as the concentration at which the spread of virus is inhibited by >95% in MT-4 human T-lymphoid cells maintained in RPMI 1640 medium containing either 10% FBS or 50% NHS. ND, not determined. Details of the assay protocols are provided in Ref. 9. Values are the geometric mean of multiple determinations. No cytotoxicity was observed for any of the compounds up to the upper limit of the assay (8.3 μM).

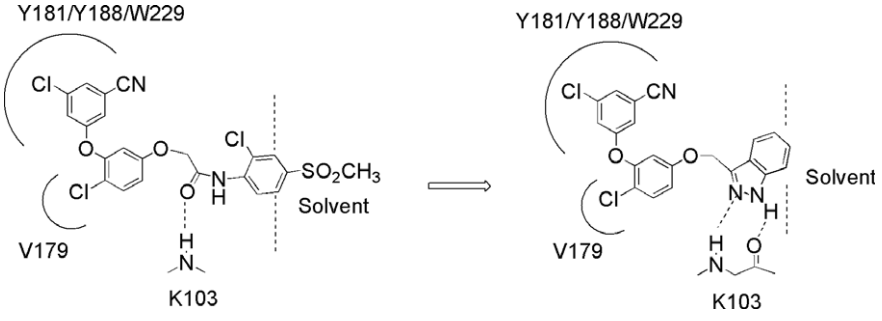

Figure 6. Proposed binding mode for indazole derivative **22**.

Table 3. Pharmacokinetic data for compound **22**

	Rat[a]	Dog[b]	Rhesus[c]
$T_{1/2}$ (h)	4.7	1.5	8.10
Cl (ml/min/kg)	13.6	28.9	24
AUC (μM h)	6.2	0.4	1.7
V_d (l/kg)	2.9	1.2	7.1
F (%)	3.3	ND	ND

[a] Average of three Sprague–Dawley rats dosed at 10 mpk po (methocel susp.) and 2 mpk iv (DMSO). All values are within 25% of the mean.

[b] Average of two beagle dogs dosed at 0.25 mpk iv (DMSO).

[c] Average of two rhesus macaques dosed at 1 mpk iv (DMSO).

the backbone of K103. The phenyl ring of the indazole makes a stacking interaction with Y318, and also appears to make lipophilic interactions with the side chains of F227, P236, and V106A. The bottom edge of this phenyl ring lies directly along the enzyme–solvent interface and appears to be amenable to further polar substitution.

In summary, we have designed and synthesized a series of novel diaryl ether based NNRTI lead structures which have excellent potency versus WT and key mutant

Table 4. Antiviral potency of compound **22** versus various clinically isolated mutant viruses (NL4-3 isolate)[a]

Mutation	IC_{50} (nM, 40% NHS)
WT	4.7
G190A	9.4
G190S	23.4
L100I	2.6
K103N	7.9
Y181C	13.8
Y188L	>1000
K101E/G190A	21
K103N/G190A	21.7
K103N/P225H	29.3
K103N/V179E	20.3
K103N/Y181C	141
Y181C/G190A	35.8
K103N/Y181C/G190A	171

[a] Compounds were analyzed in a Monogram Bioscience Phenoscreen assay in the presence of 40% NHS. The IC_{50} is defined as the concentration of compound in cell culture required to block 50% of viral replication. Details provided in Ref. 13.

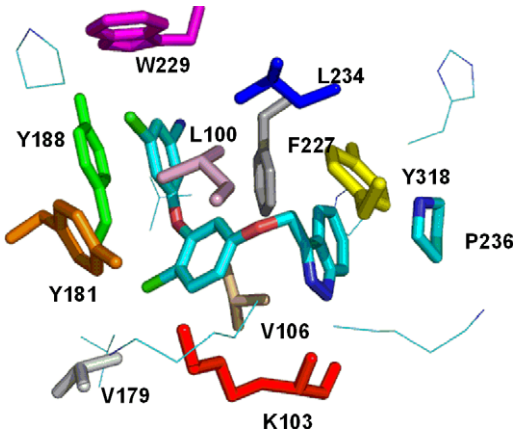

Figure 7. The X-ray crystal structure of compound **22** (blue) in the WT-NNRTI binding site (2.7 Å resolution). Details of the crystallographic studies are provided in Ref. 15.

viruses. Further systematic manipulation of the lead structures guided by SAR, modeling, and crystallography have resulted in the discovery of compound **22**, which has become the prototype of a potent and novel NNRTI platform. Synthesis in this series is continuing in an effort to modulate physical properties and prepare a more soluble and bioavailable analog of compound **22**. Taking advantage of the solvent exposed region of this molecule as a means to incorporate solubilizing groups is a key ongoing effort in our laboratories, and our further efforts in this area will be detailed in subsequent publications.

References and notes

1. Demeter, L. M.; Doamaoal, R. A. *Int. J. Biochem. Cell Biol.* **2004**, *36*, 1735.
2. Tarby, C. M. *Curr. Top. Med. Chem.* **2004**, *4*, 1045.
3. A number of groups have reported the NNRTI activity of similar structures: (a) Muraglia, E.; Kinzel, O. D.; Laufer, R.; Miller, M. D.; Moyer, G.; Munshi, V.; Orvieto, F.; Palumbi, M. C.; Pescatore, C.; Rowley, M.; Williams, P. D.; Summa, V. *Bioorg. Med. Chem. Lett.* **2006**, *16*, 2748; (b) De La Rosa, M.; Kim, H. W.; Gunic, E.; Jenket, C.; Boyle, U.; Koh, Y.; Korboukh, I.; Allan, M.; Zhang, W.; Chen, H.; Xu, W.; Nilar, S.; Yao, N.; Hamatake, R.; Lang, S. A.; Hong, Z.; Zhang, Z.; Girardet, J. *Bioorg. Med. Chem. Lett.* **2006**, *16*, 4444; (c) Gagnon, A.; Amad, M. H.; Bonneau, P. R.; Coloumbe, R.; DeRoy, P. L.; Doyon, L.; Duan, J.; Garneau, M.; Guse, I.; Jakalian, A.; Jolicoeur, E.; Landry, S.; Malenfant, E.; Simoneau, B.; Yoakim, C. *Bioorg. Med. Chem. Lett.* **2007**, *17*, 4437.
4. Romines, K. R.; Freeman, G. A.; Schaller, L. T.; Cowan, J. R.; Gonzales, S. S.; Tidwell, J. H.; Andrews, C. W.; Stammers, D. K.; Hazen, R. J.; Ferris, R. G.; Short, S. A.; Chan, J. H.; Boone, L. R. *J. Med. Chem.* **2006**, *49*, 727.
5. Compounds **2** and **3** were placed in the NNRTI binding pocket based on prior knowledge. Approximately 30 conformations of each compound were generated using two algorithms: a distance geometry (1) and a knowledge based (2) method. All conformations were then subjected to energy minimization using a distance dependent dielectric constant of 2 and applying the MMFFs forcefield (3). The depicted pose of compound **2** was chosen because it exhibited a bioactive energy conformation and the lowest overall interaction energy score as computed by MMFFs. In addition, the pose reflected the geometry shown in the poster presentation in Ref. 4 below (4). The comparison pose of compound **3** is also a low energy pose with a concomitant good overall score. In addition, it most closely resembles the pose of compound **2**. These figures were created in PyMol (5). Modeling discussion references: (1); (a) Crippen, C. M.; Havel, T. F. In *Distance Geometry and Molecular Conformation*; Bawden, E., Ed.; Research Studies Press: Wiley, New York, 1988; (b) Kuszewski, J.; Nilges, M.; Brunger, A. T. *J. Biomol. NMR* **1992**, *2*, 33; (2) Feuston, B. P.; Miller, M. D.; Culberson, J. C.; Nachbar, R. B.; Kearsley, S. L. *J. Chem. Inf. Comput. Sci.* **2001**, *41*, 754; (3) Halgren, T. A. *J. Comput. Chem.* **1996**, *17*, 490, 520, 553, 616; Halgren, T. A.; Nachbar, R. B. *J. Comput. Chem.* **1996**, *17*, 587; (4) Freeman, G.; Romines, K.; Schaller, L.; Ferris, R.; Roberts, G.; Short, S.; Weaver, K.; Hazen, R.; Creech, K.; St. Clair, M.; Tidwell, M.; Cowan, J.; Chamberlain, P.; Rena, J.; Stuart, D.; Stammers, D.; Andrews, C.; Koszalka, G.; Burnette, T.; Chan, J.; Boone, L. *Abstracts of Papers*, 2nd IAS Conference on HIV Pathogenesis and Treatment, Paris, France, July 13–16, 2003; Poster # 538; (5) PyMol, v.99 distributed by DeLano Scientific LLC was utilized to generate this image.
6. Ren, J.; Nichols, C.; Bird, L. E.; Fujiwara, T.; Sugimoto, H.; Stuart, D. I.; Stammers, D. K. *J. Biol. Chem.* **2000**, *275*, 14316.
7. Full experimental procedures and characterization data are available in the following patent application: Saggar, S. A.; Sisko, J. T.; Tucker, T. J.; Tynebor, R. M.; Su, D.; Anthony, N. J. U.S. Patent 2007/0021442, 2007; *Chem. Abstr.* **2007**, *146*, 163149.
8. Full experimental protocols for the HIV-1 RT polymerase SPA assay is described in the patent application cited in Ref. 7.
9. Vacca, J. P.; Dorsey, B. D.; Schleif, W. A.; Levin, R. B.; McDaniel, S. L.; Darke, P. D.; Zugay, J.; Quintero, J. C.; Blahy, O. M.; Roth, E.; Sardana, V. V.; Schlabac, A. J.; Graham, P. I.; Condra, J. H.; Gotlib, L.; Holloway, M. K.; Lin, J.; Chen, I.-W.; Vastag, K.; Ostovic, D.; Anderson, P. S.; Emini, E. E.; Huff, J. R. *Proc. Natl. Acad. Sci. U.S.A.* **1994**, *91*, 4096.
10. The X-ray diffraction data of the wild type RT and inhibitor **14** complex crystal were collected at 2.7 Å

resolution with R_{sym} of 0.086% and 86.4% completeness. The structure was refined to an *R*-factor of 0.168. The structure has been deposited in the PDB; PDB code is 3C6T.
11. Unpublished results, Drug Metabolism Department, Merck Research Laboratories.
12. In the paper cited in Ref. 4, there is an example of the attempted use of a benzimidazole to perform a similar function.
13. The compound was evaluated in a Monogram Bioscience PhenoSense Assay versus a panel of clinically derived RT mutants in the presence of 40% normal human serum. Values are the average of two determinations. Assays performed by Monogram Bioscience, South San Francisco, CA. Details of the assay protocols are available: http://www.monogramhiv.com/assays/hcp/phenoHIVTechnology.aspx.
14. Dykes, C.; Demeter, L. M. *Abstracts of Papers*, 14th Conference on Retroviruses and Opportunistic Infections, Los Angeles, CA, February 25–28, 2007; Poster #633.
15. The X-ray diffraction data of the wild type RT and inhibitor **22** complex crystal were collected at 2.7 Å resolution with R_{sym} of 0.103% and 93.4% completeness. The structure was refined to an *R*-factor of 0.203. The structure has been deposited in the PDB; PDB code is 3C6U.